Chinese Journal of Natural Medicines 24 (2026) 929-940

Contents lists available at ScienceDirect

Chinese Journal of Natural Medicines

journal homepage: www.cjnmcpu.com/

Original article

Patchouli alcohol protects against ulcerative colitis by alleviating ER stress and dysbiosis-mediated intestinal epithelial injury

Sha Feng[Δ], Wenhui Li[Δ], Xuqing Zhang[Δ], Qiyue Lin, Juyi Tian, Ruolin Wang, Lixia Yuan[*], Piao Luo[*], Qian Zhang[*]

Guangdong Basic Research Center of Excellence for Integrated Traditional and Western Medicine for Qingzhi Diseases, Guangdong Provincial Key Laboratory of Chinese Medicine Pharmaceutics, School of Traditional Chinese Medicine, Southern Medical University, Guangzhou 510515, China

ARTICLE INFO

Article history:
Received 31 October 2025
Revised 21 December 2025
Accepted 9 February 2026
Available online 20 August 2026

Keywords:
Ulcerative colitis
Patchouli alcohol
Protein disulfide-isomerase
Endoplasmic reticulum stress
Gut microbiota

ABSTRACT

Ulcerative colitis (UC) is defined as a chronic inflammatory disease with recurrent episodes, and current therapeutic strategies for this gastrointestinal disorder often fail to achieve satisfactory clinical outcomes. This clinical challenge underscores an urgent requirement to develop alternative treatment strategies. Patchouli alcohol (PA), a natural compound exhibiting anti-inflammatory and antioxidant properties, has shown potential; however, its precise mechanisms of action in UC remain to be fully elucidated. Our study shows that PA can effectively alleviate the symptoms of dextran sulfate sodium (DSS)-induced UC in mice. This therapeutic effect is achieved by reducing intestinal barrier impairment and inhibiting inflammatory reactions. In an LPS-induced inflammatory model using RAW264.7 cells, PA significantly downregulated the mRNA expression of *il-1β* and *il-6*. Mechanistically, protein disulfide isomerase (PDI) was identified as a direct target of PA. By inhibiting IRE1 activation *via* PDI, PA mitigates endoplasmic reticulum stress, thereby reducing intestinal epithelial injury and ultimately alleviating the severity of UC. In this research, it is determined that the ability of PA to protect the intestinal epithelial barrier is brought about by its specific targeting of PDI, which alleviates consequent endoplasmic reticulum stress and prevents cellular damage.

1. Introduction

Ulcerative colitis (UC) is defined by clinical manifestations like abdominal discomfort, watery diarrhea, and stools containing mucus and pus with blood. In some cases, it may also be accompanied by extra-intestinal manifestations including arthritis and oral ulcers. The disease most commonly affects individuals between 20 and 40 years of age. Its incidence in Asia and the Middle East is approximately 6.3 per 100 000 people, which remains lower than that in Europe and North America. However, the rate has been increasing rapidly in recent years, warranting greater clinical and public health attention [1].

The exact etiology of UC has not been fully elucidated; however, existing research suggests that its pathogenesis is closely associated with intestinal immune dysregulation, microbial dysbiosis, and antibiotic exposure [2, 3]. Under pathological conditions, impairment of the intestinal mucosal barrier and aberrant activation of the mucosal immune system contribute to a sustained inflammatory response. Current clinical management strategies include 5-aminosalicylic acid agents, glucocorticoids, and biologics such as infliximab [4-6]. Although these treatments can help alleviate clinical symptoms, none are capable of achieving a definitive cure. Consequently, given the limitations of existing therapeutic options, there is a significant need to explore novel and more effective treatment strategies.

Patchouli alcohol (PA)—a tricyclic sesquiterpene isolated from the traditional Chinese medicinal plant *Pogostemon cablin*—possesses a diverse array of pharmacological properties, ranging from anti-inflammatory and antiviral effects to anti-*Helicobacter pylori* and antitumor activities [7, 8]. UC is an intestinal disorder characterized by a complex pathogenesis involving multiple key factors, such as impairment of the intestinal epithelial barrier, aberrant immune activation, and dysbiosis of the gut microbiota. Consequently, effective therapeutic strategies must target these diverse pathological mechanisms. Previous studies [9, 10] have demonstrated that PA significantly attenuates the inflammatory response, preserves intestinal epithelial barrier integrity, suppresses cell death signaling pathways, and reduces tryptophan catabolism in a dextran sulfate sodium (DSS)-induced mouse model of acute colitis. In addition, it has been reported that PA effectively delays inflammatory progression in UC mice by inhibiting the HO-1 and iNOS-related antioxidant signaling pathways, without markedly altering the composition of the intestinal microbiota [11]. These findings collectively indicate that PA holds promise as a potential therapeutic agent for ulcerative colitis. Nevertheless, its precise molecular targets and mechanisms of action remain incompletely elucidated, warranting further in-depth investigation.

As a pivotal endoplasmic reticulum-resident enzyme, protein disulfide isomerase (PDI) catalyzes the formation, cleavage, and rearrangement of disulfide bonds within target proteins,

* Corresponding author.
E-mail addresses: cnylxtcm@163.com (L. Yuan); luopiao@smu.edu.cn (P. Luo); zhangqian408@smu.edu.cn (Q. Zhang)
Δ These authors contributed equally to this work.

https://doi.org/10.1016/S1875-5364(26)61194-6

thereby facilitating the correct folding of newly synthesized polypeptide chains. Its versatility stems from its diverse enzymatic activities, including oxidoreductase activity, molecular chaperone activity, and S-nitrosylation activity, which enable it to participate in and regulate several cellular physiological processes. The molecular structure of PDI contains four thioredoxin-like structural domains, a, a′, b, and b′, as well as an acidic C-terminal extension region and an X linker region connecting the b′ and a′ structural domains [12, 13]. Among them, the a and a′ domains are catalytically active and are the core regions of disulfide bond heterodimerization reactions. The b′ domain is mainly responsible for recognizing and binding substrate proteins due to its highly conserved features [14], as well as the targets of various PDI inhibitors [15, 16]. The b domain and the X linker indirectly affect the interaction with substrates by regulating the degree of opening of the overall conformation of PDI. The synergistic effect between these structural domains makes PDI play a key role in maintaining protein homeostasis, and its aberrant function is closely related to a variety of diseases, including cancer [17], neurodegenerative diseases [18, 19], etc. So PDI has also become an important target for therapeutic research of related diseases.

In the pathogenesis and progression of UC, endoplasmic reticulum stress (ER stress) and its mediated unfolded protein response (UPR) have been validated as one of the key pathogenic drivers, which not only modulate intestinal epithelial cell survival and gut barrier integrity, but also further amplify local inflammatory responses, thereby contributing to disease onset and persistence [20, 21]. Aberrant protein misfolding and subsequent aggregation within the endoplasmic reticulum can initiate the unfolded protein response (UPR). This response aims to restore endoplasmic reticulum homeostasis by enhancing molecular chaperone expression, inhibiting protein translation and promoting degradation or refolding of misfolded proteins. PDI is capable of changing its conformation *via* post-translational modifications like phosphorylation. thus switching from a typical “folding enzyme” function to a “retention enzyme” activity, which effectively prevents the disaggregation of proteins and maintains partial folding of proteins [22, 23]. In addition, PDI can interact directly with core UPR signaling molecules (e.g. IRE1) and negatively regulate its phosphorylation level, thus regulating the strength of UPR signaling pathway [19, 23]. On the other hand, PDI interacts with endoplasmic reticulum oxidizing reductase 1 (ERO1) enzyme, which is an essential component of the ERO1 redox environment in the endoplasmic reticulum lumen. Yet, when stress is intense or prolonged, excessive activation of the PDI–ERO1 axis could result in an overabundance of reactive oxygen species (ROS), which not only exacerbates endoplasmic reticulum stress, but also promotes the onset and development of inflammatory responses [24]. In summary, PDI is involved in the regulation of endoplasmic reticulum stress through multiple molecular mechanisms, and the dynamic change of its functional status has a decisive impact on cell fate. Based on the central position of PDI in endoplasmic reticulum quality control and stress response, targeted regulation of PDI may provide a new intervention strategy for the treatment of ulcerative colitis by remodeling endoplasmic reticulum homeostasis and alleviating the over-activation of UPR.

In this study, we identified PDI as a direct target of PA using a combination of database screening and proteomic analysis, combined with experimental methods such as drug affinity response targeted stability (DARTS). PDI, as a key regulator in the endoplasmic reticulum stress pathway, plays a central role in the maintenance of protein homeostasis and cellular stress response. However, its potential involvement in the pathological progression of UC *via* modulation of the ER stress pathway remains to be elucidated. Based on the potential ability of PA to target PDI and possibly modulate inflammation and ER stress, the present study further delves into the mechanism of PA’s action in the context of UC, aiming to provide a new theoretical basis and potential strategy for UC.

2. Materials and methods

2.1. Chemical reagents

PA (purity ≥ 98%, CAS: 5986-55-0) and DSS (CAS: 9011-18-1) were procured from Bethealth People Biomedical Technology (Beijing, China). LPS (L2880) was obtained from Sigma-Aldrich (Shanghai, China). Specific primary antibodies, including PDI (66422-1-Ig), IRE1/ERN1 (27528-1-AP), XBP1S (24868-1-AP), β-actin (20536-1-AP), occludin (66378-1-Ig), CHOP/GADD153 (152044-1-AP), GAPDH (60004-1-Ig), and GRP78/BIP (11587-1-AP), were purchased from Proteintech (Hubei, China). E-cadherin (A20798), claudin-4 (A23841), and ZO-1 (A0659) were from ABclonal (Hubei, China). AF488-labeled goat anti-rabbit IgG (H + L) (A0423), AF647-labeled goat anti-mouse IgG (H + L) (A0473), and Hoechst 33342 (C1028) were purchased from Beyotime Biotechnology (Shanghai, China).

2.2. Cell culture and treatment

The RAW264.7 (ATCC® TIB-71™) and the Caco2 cell line (ATCC® HTB-37™) were obtained from the American Type Culture Collection (ATCC) and authenticated by short tandem repeat (STR) profiling prior to use.

For Caco2 cell culture and experimental grouping: cells were seeded in 6-well plates at a density of 5×10^5 cells/well and cultured in Minimum Essential Medium (MEM, PM150410, Procell, Wuhan, China) supplemented with 20% Fetal Bovine Serum (FBS, FSP500, Excell, Suzhou, China) and 1% PS (15140122, Gibco, Massachusetts, USA) in a humidified incubator with 5% CO_2 at 37 °C. After 24 h of adherent growth (confluency reached about 80%). The trans-epithelial electrical resistance (TEER) was measured daily using the RE1600 Epithelial Cell Voltage-Resistance Meter (RE1600, Kingtech, Beijing, China), and a resistance value greater than 500 $\Omega \cdot cm^2$ was considered indicative of the formation of a monolayer barrier. The specific grouping is as follows: (1) Control group: no LPS induction or PA treatment; (2) LPS group: induced with 2 $\mu g \cdot mL^{-1}$ LPS for 24 h; (3) PA groups: pre-induced with 2 $\mu g \cdot mL^{-1}$ LPS for 24 h, followed by treatment with different concentrations of PA (25 and 50 $\mu mol \cdot L^{-1}$; purity ≥ 98%, WKQ-0000074, Beite Renkang, Beijing, China) for another 24 h. Following the completion of all experimental interventions, cellular samples were washed with pre-cooled phosphate-buffered saline (6125285, Gibco, Massachusetts, USA), and total proteins were extracted using RIPA lysis buffer (P0013B, Beyotime, Shanghai, China) supplemented with 1% protease inhibitor (PI, P1006, Beyotime, Shanghai, China) for Western blot (WB) analysis; total RNA was isolated using the cell/tissue total RNA kit (19221ES50, Yisheng, Shanghai, China) for quantitative real-time polymerase chain reaction (RT-qPCR) to detect the expression of tight junction-related genes, aiming to evaluate the protective effect of PA on LPS-induced intestinal epithelial barrier dysfunction.

For RAW264.7 cell culture and experimental grouping: cells were seeded in 6-well plates at a density of 1×10^6 cells/well and cultured in Dulbecco’s Modified Eagle Medium (DMEM, C11995500BT, Gibco, China) under the same incubator conditions as Caco2 cells. After 12 h of adherent growth, the cells were subjected to the following treatments: (1) Control group: no LPS induction or PA treatment; (2) LPS group: induced with 100 $ng \cdot mL^{-1}$ LPS for 3 h; (3) PA groups: after undergoing the same treatment as the LPS group, the cells were further treated with PA at the same concentrations (25 and 50 $\mu mol \cdot L^{-1}$) as Caco2

cells for 24 h. After treatment, cells were harvested by centrifugation (800 r·min^{-1}, 5 min) following PBS washing, and total proteins/RNA were extracted as described above for WB and RT-qPCR analysis, which was designed to explore whether PA modulates LPS-induced macrophage activation, inflammatory response and ER stress.

All experiments were conducted in three independent replicates to ensure experimental reproducibility and cells were passaged no more than 10 times to ensure consistent biological activity.

2.3. Animals

The male C57BL/6 mice (6 weeks old, weighing between 18 and 22 g, specific pathogen-free) were purchased from Guangdong Zhiyuan Biomedical Technology Co., Ltd. [License No. SCXK (Guangdong) 2023-0066]. All experimental animals were maintained in standardized housing environments with a temperature regulated at 22–24 °C, a 12-h light/dark cycle, and relative humidity kept at 50%–60%. Standard diet and sterile water were provided to all mice.

After a one-week acclimatization phase, the mice were randomly allocated into four groups (Ctrl, DSS, PA-L, and PA-H), with 5 mice per group. Among them, the DSS, PA-L and PA-H groups were free to drink 3% DSS water for 7 d and then switched to sterile water, while the Ctrl group was free to drink sterile water from the beginning to the end. The PA-L and PA-H groups were gavaged daily with 20 and 40 mg·kg^{-1} of PA, respectively, from day 1 to day 10 of the experiment.

Since the initiation of the experiment, the body weight of mice was recorded daily, and fecal samples were collected synchronously for the observation of fecal morphology and determination of fecal occult blood (BC8271, Solarbio, Beijing, China), with specific scoring criteria detailed in Section 2.5. Ultimately, isoflurane was administered *via* inhalation to anesthetize the animals, with induction performed at 4%–5% and maintenance sustained at 1.5%–2.5%. After the complete disappearance of the paw pinch reflex, 0.5 mL of blood was collected by enucleation; subsequent to blood collection, mice were euthanized by cervical dislocation for colon sampling. The colon was defined as the segment from the cecum to 1 cm above the rectum. Following sampling, photographs were taken and the length was measured. The colon tissue, excluding the cecum, was divided into 3 equal parts: one part was fixed in paraformaldehyde for subsequent paraffin section preparation; the other two parts were first subjected to internal feces collection, thoroughly rinsed, and then cryopreserved for subsequent WB analysis.

All experimental procedures involving animals were approved by the Animal Experiment Center of Shenzhen People's Hospital (Ethical Approval No. AUP-240802-WJG-651-01).

2.4. Disease activity index

The DAI score was based on the following three items: percentage weight loss, fecal character, and blood in stool. The grading and scoring of weight loss were defined as 0% (0 point), 1%–5% (1 point), 5%–10% (2 points), 10%–15% (3 points), > 15% (4 points); formed stools (0 point), loose stools (1 point), mucous stool (2 points), watery stools (3 points); stools with negative occult blood (0 point), stools with positive occult blood (1 point), slightly bloody stools in the naked eye (2 points), and severe bloody stools in the naked eye (3 points), respectively. The DAI score was the sum score of three parts (mucous stool = stools were unformed and soft without adherence to the perianal region; watery stool = watery stool that sticks to the anus; slight bloody stool to the naked eye = blood in the stool; and severe blood in the stool = blood in the anus).

2.5. HE staining, AB/PAS staining and PAS staining

Colonic tissues were fixed overnight by paraformaldehyde and then embedded in paraffin and sectioned as described previously [25]. Tissue morphology was observed and scored after hematoxylin-eosin staining. Similarly, colon sections were stained with AB/PAS staining or PAS staining used to assess changes in colonic mucus thickness and number of goblet cells per crypt.

2.6. HE staining scoring criteria

Inflammatory cell infiltration (no infiltration: 0 point; infiltration of glandular base: 1 point; infiltration of muscularis mucosae: 2 points; extensive infiltration of muscularis mucosae: 3 points; infiltration of submucosa: 4 points); edema degree (no edema: 0 point; mild edema: 1 point; moderate edema: 2 points; severe edema: 3 points); crypt damage (no damage: 0 point; slight loss of goblet cells: 1 point; massive loss of goblet cells: 2 points; slight loss of crypts: 3 points; massive loss of crypts: 4 points); ulceration (no ulcer: 0 point; involvement of lamina propria: 1 point; involvement of submucosa: 2 points; transmural ulcer: 3 points).

2.7. Immunofluorescence

After colon paraffin sections were deparaffinized and antigenically repaired as previously described [26]. The tissue sections were left to incubate with primary antibodies—such as anti-ZO-1 (A0659, ABclonal, Wuhan, China), anti-occludin (66378-1-Ig, Proteintech, Wuhan, China), and anti-E-cadherin (A20798, ABclonal, Wuhan, China) at 4 °C overnight. Subsequently, the sections were incubated with secondary antibodies of AlexaFluor488 (A0423, Beyotime, Shanghai, China) and AlexaFluor647 (A0473, Beyotime, Shanghai, China) respectively, for 2 h at room temperature protected from light. All samples were stained for nucleus with Hoechst 33342 (C1028, Beyotime, Shanghai, China). Finally, the resulting fluorescence signals were examined using a fluorescence microscope (Leica TCS-SP8-SR, Wetzlar, Germany).

2.8. Real-time PCR analysis

Total RNA was extracted using the cell/tissue total RNA kit (19221ES50, Yisheng, China). 1st strand cDNA synthesis kit (11121ES60, Yisheng, China) removes residual genome from cellular RNA samples and reverse transcribes the samples into cDNA for subsequent use. Lastly, the assay was carried out using qPCR SYBR green master mix (11201ES08, Yisheng, China) on a CFX96 real-time fluorescent quantitative PCR detection system (Applied Biosystems). To measure the relative expression level of the target gene, *gapdh* and *β-actin* were chosen as internal controls. We used $2^{-\Delta\Delta CT}$ calculation to present the experimental results. The primer sequences used in this study are detailed in Table S1.

2.9. Proteome analysis

The colon tissue proteins were initially denatured using 8 mol·L^{-1} urea, and 100 μg of protein was then aliquoted for subsequent enzymatic digestion. The denatured proteins were reduced using 20 mmol·L^{-1} dithiothreitol (DTT, D9779, Sigma-Aldrich, Shanghai, China), followed by alkylation with 40 mmol·L^{-1} iodoacetamide (IAA, I1149, Sigma-Aldrich, Shanghai, China) to block free thiol groups. Subsequently, a trichloroacetic acid (TCA, T104261, Aladdin, China) solution was introduced to achieve further denaturation and protein precipitation. Following collection and re-solubilisation of the precipitate, lysyl endopeptidase (LysC) (1∶50, LYSC9001, Sigma-Aldrich, China) and trypsin (1∶50, V5111, Promega, USA) were added. The mixture was then incub-

ated in order to cleave proteins into peptide fragments. Ultimately, the samples of digested peptides were subjected to a process of desalting and purification. The processed samples were then subjected to mass spectrometry (MS, Thermo Scientific, USA) for detection and proteomic analysis.

2.10. Western blot

Total protein isolates from cultured cells or tissue samples were obtained *via* RIPA lysis buffer containing 1% protease inhibitors, and their concentrations were subsequently equalized using a BCA protein assay kit (23227, Thermo Scientific, Massachusetts, USA). Different concentrations of SDS-PAGE were selected according to the molecular weight of the target proteins for protein separation, following electrophoretic transfer to PVDF membranes, which were sectioned after 1 h of BSA block. Subsequent incubation with the relevant primary antibodies was performed at 4 °C for more than 16 h. The primary antibodies were as follows: PDI (66422-1-Ig, proteintech, Wuhan, China), IRE1 (27528-1-AP, Proteintech, Wuhan, China), BIP (11587-1-AP, Proteintech, Wuhan, China), XBP1s (24868-1-AP, Proteintech, Wuhan, China), GAPDH (60004-1-Ig, Proteintech, Wuhan, China), β-actin (20536-1-AP, Proteintech, Wuhan, China), E-cadherin (A20798, ABclonal, Wuhan, China), occludin (66378-1-Ig, Proteintech, Wuhan, China), and claudin-4 (A23841 ABclonal, Wuhan, China). HRP-conjugated secondary antibodies utilized in this study included goat anti-rabbit IgG (H + L) (SA00001-2, Proteintech, Wuhan, China) and goat anti-mouse IgG (H + L) (RGAM011, Proteintech, Wuhan, China). On the next day, the bands were incubated with HRP-coupled secondary antibody and exposed with ECL kit (35055, Thermo Fisher, Massachusetts, USA), and the gray values of the bands were counted by ImageJ (Version 1.53a, National Institutes of Health, Bethesda, Maryland, USA).

2.11. CO-IP-Western blot

Total proteins were extracted from RAW264.7 cells with IP lysis buffer composed of 25 mmol·L^{-1} Tris-HCl (pH 7.4, T1270, Solarbio, China), 150 mmol·L^{-1} NaCl (S805277, Macklin, China), 1% NP-40 (AN8032, ACMEC, China), 5% glycerol (BS154, Biosharp, China) and 1% PI. For each group, 3 mg of protein was reserved for subsequent co-immunoprecipitation (Co-IP) assays, and an additional 20 μg of protein was set aside as the input sample. To eliminate non-specific binding interference, each sample was supplemented with 10 μL of protein A/G beads (88803, Thermofisher, Massachusetts, USA), and incubation was performed at room temperature for 30 min. After centrifugation, the supernatants were collected. Subsequently, 2 μg of IgG antibody (30000-0-AP, Proteintech, Wuhan, China) was added to the IgG control group, while an equal amount of PDI antibody (11245-1-AP, Proteintech, Wuhan, China) was added to the remaining experimental groups. All samples were incubated overnight at 4 °C. Upon completion of incubation, 15 μL of pre-washed A/G beads were added to each group, and continuous incubation was performed at 4 °C for 1 h to capture the antigen-antibody complexes. The complexes were then washed 3 times with IP lysis buffer containing 1% PI. Next, 15 μL of 2 × loading buffer (P0015L, Beyotime, Shanghai, China) was added, and the samples were boiled at 95 °C for 10 min to denature the proteins. After centrifugation, the supernatants were collected for Western blot analysis, and the remaining operational steps were performed in accordance with the method described in Section 2.10.

2.12. Insulin reduction assay

PDI is used as a reductant to cleave the disulfide bonds of insulin, causing it to denature, aggregate, and form a precipitate; the reduction activity is then reflected by measuring the increase in solution absorbance. This experiment was performed following a previously established protocol [27]. 25 and 50 μmol·L^{-1} PA was incubated with either RAW264.7 cell lysate or 0.5 mmol·L^{-1} purified PDI protein at room temperature for 30 min. Subsequently, a premixed solution containing 130 mmol·L^{-1} insulin (PB180432, Procell, China), 2.5 mmol·L^{-1} EDTA (AM9260G, Invitrogen, USA), 0.5 mmol·L^{-1} DTT and 0.1 mol·L^{-1} PBS (pH 7.5) was supplemented, and the mixture was incubated at room temperature for 20 min. Upon completion of the reaction, the absorbance (OD value) of the reaction solution was measured at 650 nm using a microplate reader.

2.13. Drug affinity responsive target stability (DARTS)

DARTS is a label-free target identification technique, it relies on "small molecule-target protein binding enhancing the protein's resistance to protease hydrolysis" to identify potential targets *via* protease treatment and electrophoresis. First, following the collection of cellular samples, whole protein isolates were prepared utilizing NP-40 lysis buffer. The extracted protein solution was split into two equal aliquots: one was treated with DMSO (as the control) and the other with PA (as the treatment group), and both were incubated for 1 h under appropriate conditions. Upon completion of the reaction, each group of proteins was further divided into 6 equal aliquots, which were then incubated with gradient concentrations of pronase (10165921001, Roche) (1/4000−1/250, *W/W*) for 15 min. The reaction was terminated by adding loading buffer and boiling the samples. Subsequent experimental procedures were performed in accordance with the standard Western blot protocol.

2.14. 16S rRNA sequencing

Mouse fecal samples were collected and sent to NovaSeq for library construction and sequencing analysis. Similar to the previous procedure, specific primers (341F: CCTAYGGGRBGCASCAG; 806R: GGACTACNNGGGTATCTAAT) were employed to amplify the V3-V4 segment of bacterial 16S rDNA. Afterward, the PCR amplicons were sequenced using the NovaSeq platform to assess the abundance of bacteria.

2.15. Public database data retrieval and analysis

The clinical data were retrieved from the public Gene Expression Omnibus (GEO) database (https://www.ncbi.nlm.nih.gov/geo/) under the accession number GSE179285, which encompasses intestinal biopsy specimens from patients with IBD, including Crohn's disease (CD) and UC, as well as healthy control individuals. The dataset includes a total of 177 CD patients, 94 UC patients, and 58 healthy controls, with biopsy tissues collected from the terminal ileum and colon, covering active lesions, inactive adjacent mucosa, and normal intestinal tissues from healthy individuals; total RNA isolated from these biopsy samples was hybridized to Agilent human 4 × 44K v1 microarrays using a dual-channel approach with a universal reference sample, enabling genome-wide gene expression profiling. This dataset was employed to identify gene expression differences between active and inactive intestinal tissues in IBD patients, aiming to characterize the molecular heterogeneity of active disease and provide molecular evidence for subsequent analyses.

Given that our investigation centered on the genes exhibiting differential expression profiles between healthy individuals and UC patients, we further compared their gene expression data, aiming to characterize the molecular heterogeneity of active disease by analyzing gene expression differences between active and inactive intestinal tissues in IBD patients and to provide molecu-

lar evidence for subsequent analyses. Statistical comparisons between groups were performed using the Mann-Whitney U test, and the results are presented as mean ± SEM.

2.16. Statistical analysis

The results of this study are presented as mean ± standard error (SEM) for *in vivo* experiments ($n \geq 4$) and *in vitro* experiments ($n \geq 3$). Statistical comparisons across multiple groups were performed using one-way ANOVA with Tukey-Kramer post hoc testing. Statistical comparisons between two groups, the Mann-Whitney U test was applied for non-normally distributed data. Two-way ANOVA with Tukey's multiple comparisons test was performed to analyze repeated measures data. Statistical analyses were performed by GraphPad Prism 10.1.2. Heat maps illustrating the correlation between intestinal flora and colonic parameters were generated using R project (4.5.1 version). Statistical significance: $^{*}P < 0.05$, $^{**}P < 0.01$, $^{***}P < 0.001$, $^{****}P < 0.0001$ *vs* DSS or LPS group; ns, not significant.

3. Results

3.1. Treatment with PA attenuates colon damage in mice exposed to DSS

In accordance with the experimental protocol and dosing schedule outlined in Fig. 1A, we performed animal experiments while monitoring the body weight, fecal morphology, and presence of blood in stools of mice on a daily basis. Body weight loss serves as a key indicator of UC progression. Consistent with our expectations, mice in the DSS group exhibited significant weight loss during the late phase of treatment. Notably, both low and high dose PA treatment effectively reversed DSS induced body weight loss, and the body weight change curves of the two treatment groups nearly overlapped (Fig. 1B). Additionally, DSS exposure induced diarrhea and hematochezia in mice, leading to a marked elevation in the disease activity index (DAI) score. In contrast, mice treated with PA showed alleviation of these symptoms (Fig. 1C). Importantly, colon shortening is a hallmark manifestation of colitis. This pathological change was prominent in the DSS group, whereas PA treatment exerted a notable inhibitory effect on colon shortening (Figs. 1D and 1E).

The colonic epithelium of healthy individuals is defined by structural integrity, a well-organized mucus layer, and a balanced intestinal microbiota—all of which collectively maintain intestinal homeostasis. In contrast, UC is characterized by disruption of colonic architecture, loss of goblet cells, and infiltration of inflammatory cells. Histological analysis of HE-stained colonic sections showed that mice in the DSS group displayed severe damage to the epithelial barrier, atrophy of intestinal villi, submucosal edema, and extensive inflammatory cell infiltration. By comparison, both the PA-L and PA-H groups exhibited relatively preserved epithelial structure and reduced inflammatory infiltration. Goblet cells are critical for secreting the protective mucus layer that defends the colonic epithelium. A decrease in goblet cell numbers impairs mucus production, thereby enhancing intestinal susceptibility to pathogenic bacteria. AB/PAS and PAS staining further verified a marked depletion of goblet cells in mice administered DSS, and this depletion was notably reversed by PA treatment (Figs. 1G–1I).

In summary, these results demonstrate that PA administration significantly mitigates symptoms of DSS-induced acute colitis. Furthermore, PA promotes the restoration of intestinal barrier integrity and the recovery of goblet cell populations.

3.2. PA alleviates DSS-induced intestinal barrier damage

Given that HE-stained sections revealed significant structural impairment of the intestinal barrier in DSS-treated mice, we further assessed intestinal epithelial barrier integrity *via* immunofluorescence staining of key tight junction-associated proteins. Through immunofluorescent visualization, the fluorescent signals of tight junction proteins ZO-1, occludin, and E-cadherin in the colonic mucosa were found to be significantly weakened in DSS-treated mice relative to the control group. Notably, following PA treatment, the fluorescence signals of these proteins were significantly enhanced, suggesting that PA facilitates the restoration of epithelial integrity (Figs. 2A and 2B).

Consistently, the abundance of E-cadherin and claudin-4 proteins was markedly reduced in colonic samples from mice with DSS-induced colitis. Following PA treatment, the expression of these tight junction-related proteins was upregulated to varying degrees—demonstrating that PA can partially reverse DSS-induced loss of tight junction proteins (Figs. 2C–2E). Notably, the high-dose PA group showed more pronounced recovery, which implies a dose-dependent therapeutic effect of PA.

3.3. PA exhibits barrier-protective and anti-inflammatory effects *in vitro*

Given that Caco-2 cells spontaneously differentiate into intestinal epithelial-like cells under *in vitro* culture conditions, this study employed a Caco-2 monolayer model to simulate the intestinal epithelial barrier. Barrier integrity was evaluated by measuring TEER, with a TEER value exceeding 500 $\Omega \cdot cm^2$ indicating complete monolayer differentiation (Fig. S1A). We first performed CCK-8 assays to evaluate the cytotoxicity of PA (0–200 $\mu mol \cdot L^{-1}$) in Caco-2 cells. The results demonstrated that PA was non-cytotoxic and safe for Caco-2 cells within this concentration range (Fig. 3A). Western blot analysis showed that LPS treatment significantly reduced E-cadherin protein expression, while subsequent treatment with PA partially restored its expression (Figs. 3B–3E). RT-qPCR results demonstrated that PA partially attenuated the LPS-induced downregulation of *e-cadherin* and *claudin-4* mRNA expression (Figs. 3E and 3F).

Additionally, CCK-8 assays were performed on RAW264.7 cells treated with PA (0–400 $\mu mol \cdot L^{-1}$), revealing an IC_{50} value of 206.4 $\mu mol \cdot L^{-1}$ (Fig. S1B). 50 $\mu mol \cdot L^{-1}$ PA was chosen to further examine its modulation of inflammatory cytokine gene expression *via* RT-qPCR. In the RAW264.7 macrophage cell line, LPS stimulation significantly upregulated the mRNA expression of the pro-inflammatory cytokines *il-6* and *il-1β*. In contrast, PA treatment markedly suppressed the expression of these two cytokines (Figs. 3H and 3I). Taken together, these results demonstrate that PA not only exerts a protective effect on the intestinal epithelial barrier *in vitro* but also exhibits significant anti-inflammatory activity. These findings suggest that PA may alleviate UC through multiple pharmacological mechanisms, including enhancing intestinal epithelial barrier integrity and suppressing inflammatory responses.

3.4. PA modulates the endoplasmic reticulum stress pathway to exert a protective effect against UC

To clarify the precise molecular mechanisms through which PA exerts its protective effects, quantitative proteomic analysis was conducted on colon tissues obtained from the experimental mice (Fig. 4A). In comparison with the control group, animals administered DSS displayed 444 upregulated and 468 downregulated proteins. In contrast, PA administration significantly attenuated these proteomic alterations: compared to the DSS group,

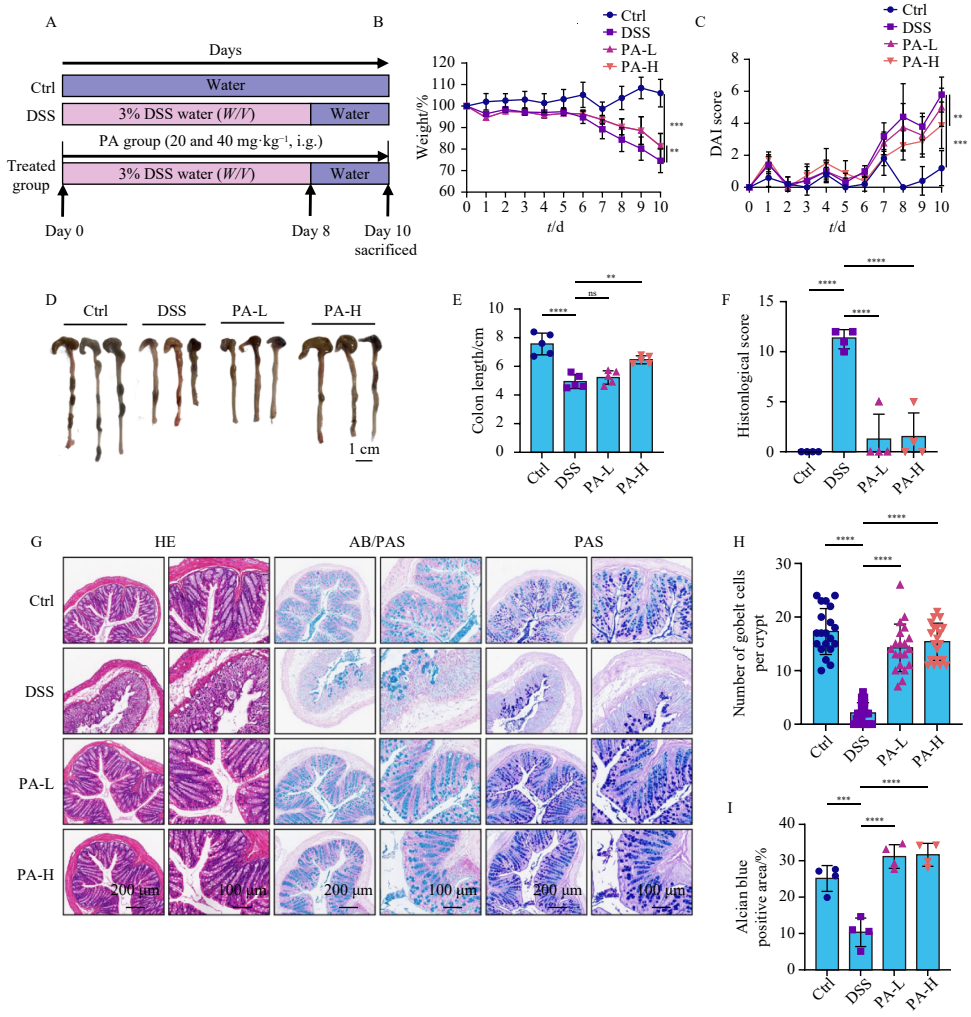

Fig. 1 PA alleviates the symptoms of DSS-induced experimental colitis in mice. (A) Flow chart of animal experimental drug administration. (B) Body weight changes of mice in each group. (C) DAI scores of mice in each group. (D) Representative colon diagram from each group (scale bar = 1 cm). (E) Quantitative analysis of colon length in each group. (F) Histochemical scores of colon HE-stained sections. (G) Representative histopathological staining of colon tissues: HE staining (assessing tissue structure), Alcian blue/periodic acid-Schiff (AB/PAS) staining, and PAS staining (both evaluating goblet cell mucus secretion; scale bars = 200 μm for low-magnification fields, 100 μm for high-magnification fields). (H) Quantitative analysis of goblet cell number per crypt. (I) Quantitative of the AB/PAS positive areas. All experiments were performed with at least 4 mice per group (n = 4–20). Data were statistically analyzed using Two-way ANOVA (B and C). Statistical analysis was performed using one-way ANOVA to compare differences among multiple groups, followed by Tukey's honestly significant difference post-hoc test to determine pairwise differences between groups (E, F, H and I). Data are presented as mean ± SEM. Statistical significance: $^{*}P < 0.05$, $^{**}P < 0.01$, $^{***}P < 0.001$, $^{****}P < 0.0001$ *vs* DSS; ns, not significant.

371 proteins were upregulated and 439 were downregulated, indicating a substantial reversal of DSS-induced proteomic changes (Fig. 4B). The heatmap revealed widespread protein dysregulation in the colitis model group, which was reversed by PA treatment; key changes involved proteins linked to oxidative stress, inflammation, ER stress, and intestinal barrier function (Fig. S2A).

Subsequent functional enrichment assessments verified that the variably expressed proteins were prominently concentrated across numerous biological signaling pathways. Specifically, PA treatment markedly upregulated proteins involved in acetyl-CoA metabolism, intestinal epithelial absorption, and glycolysis. In contrast, pathways related to inflammatory response, protein folding, and endoplasmic reticulum stress were significantly downregulated (Fig. 4C). Consistent with this trend, the endoplasmic reticulum stress-related protein BIP also showed a corresponding change in enrichment degree (Fig. 4D). These results suggest that PA may mitigate colonic tissue damage by enhancing epithelial energy metabolism and nutrient absorption, while concurrently attenuating intestinal inflammation and endoplasmic reticulum stress.

Moreover, we detected significant changes in how key tight junction-related proteins are expressed, such as occludin and multiple members of the claudin family (claudin-3 and claudin-15), and these proteins were significantly modulated following PA treatment (Figs. 4E–4H). These results are consistent with our previous *in vivo* and *in vitro* findings, which demonstrated that PA effectively mitigates DSS-induced intestinal barrier impairment and restores tight junction protein expression. This further confirms PA's protective role in preserving epithelial barrier integrity.

Notably, this study also identified PA's potential regulation of PDI expression levels (Fig. 4I). In the LPS/DSS-induced inflammatory model, a trend of increased PDI expression upon inflammatory stimulation and a slight decrease following PA intervention was only observed in RAW264.7 macrophages, and this decreasing trend did not reach statistical significance ($P > 0.05$). Collectively, PA did not exert a significant regulatory effect on the protein expression level of PDI (Figs. S2B–S2G). As a multifunctional enzyme, PDI serves a pivotal function in the processes of protein folding and quality surveillance within the endoplasmic reticulum. Unexpectedly, in the present experimental model, PA failed to exert the anticipated regulatory effect on the protein expression level of PDI. This finding prompted us to further investigate the pharmacological mechanism by which PA modulates ER stress pathways *via* PDI mediation.

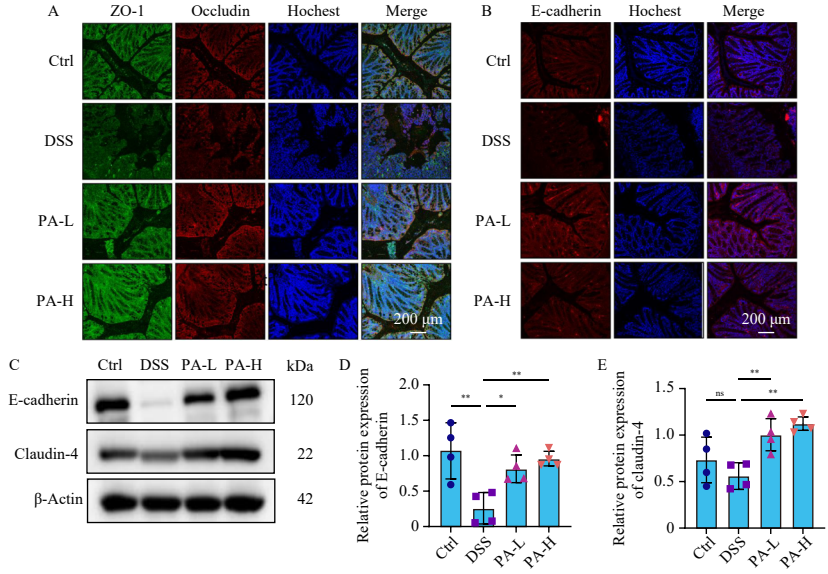

Fig. 2 PA ameliorates intestinal mucosal barrier impairment elicited by DSS in mice. (A) Immunofluorescence staining of colon tissue sections showing the distribution of tight junction proteins ZO-1 (green) and occludin (red), with nuclei counterstained by Hoechst (blue); merged images display co-localization (scale bar = 200 μm). (B) Immunofluorescence staining of colon tissue sections showing the distribution of adherens junction protein E-cadherin (red), with nuclei counterstained by Hoechst (blue); merged images display E-cadherin localization (scale bar = 200 μm). (C) WB bands of E-cadherin, claudin-4, and internal reference β-actin in colon tissue lysates. (D and E) WB quantitative analysis of E-cadherin (D) and claudin-4 (E). All experiments were conducted with at least 3 independent replicates per group. Statistical analysis was performed using one-way ANOVA followed by Tukey's post-hoc test. Data are presented as mean ± SEM. Statistical significance: $^{*}P < 0.05$, $^{**}P < 0.01$, $^{***}P < 0.001$, $^{****}P < 0.0001$ *vs* DSS group; ns, not significant.

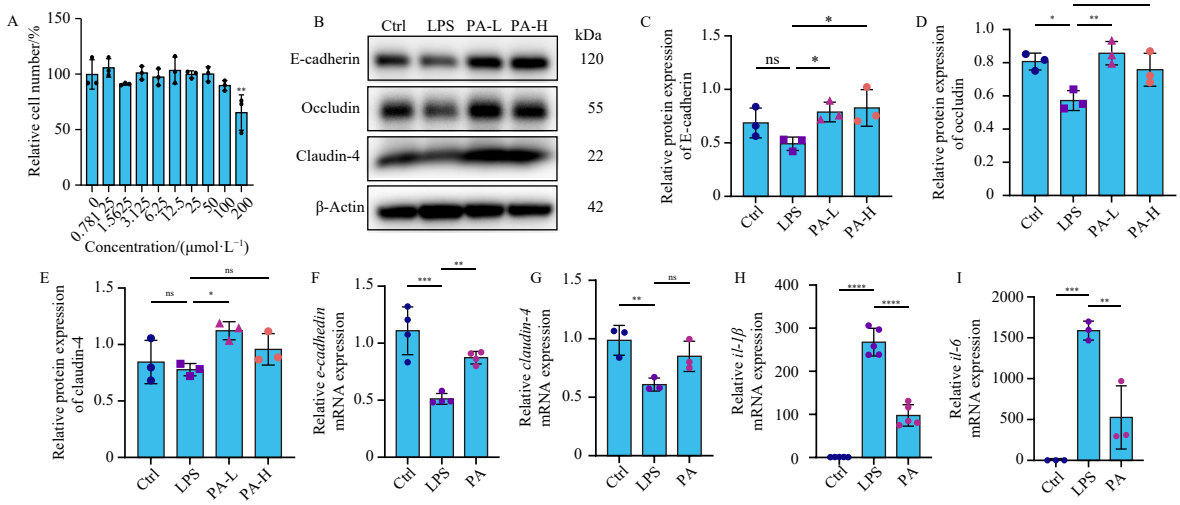

Fig. 3 *In vitro* improvement of LPS-induced Caco2 cell barrier damage by PA. (A) Relative cell number of Caco2 cells after 24 h treatment with PA at concentrations ranging from 0 to 200 μmol·L^{-1}. (B) WB bands of E-cadherin, occludin, claudin-4 and internal reference β-actin in Caco2 cells (PA-L, 25 μmol·L^{-1}; PA-H, 50 μmol·L^{-1}). (C–E) Quantitative analysis of WB results for claudin-4 (C), occludin (D), and claudin-4 (E) protein expression. (F and G) RT-qPCR analysis of *e-cadherin* (F) and *claudin-4* (G) mRNA expression in Caco2 cells (PA : 50 μmol·L^{-1}). (H and I) RT-qPCR analysis of pro-inflammatory cytokine mRNA expression: *il-1β* (H) and *il-6* (I) in RAW264.7 cells (PA: 50 μmol·L^{-1}). All experiments were performed with at least 3 independent replicates (n = 3–5). Data were statistically analyzed *via* one-way ANOVA with subsequent Tukey's multiple comparisons test. Data are presented as mean ± SEM. Statistical significance: $^{*}P < 0.05$, $^{**}P < 0.01$, $^{***}P < 0.001$, $^{****}P < 0.0001$ *vs* LPS group; ns, not significant.

3.5. PDI is a targeted agent for PA in alleviating UC

We first verified the effect of PA on PDI *in vitro*. As a label-free target screening technique, DARTS has a core advantage that the specific drug-target protein binding endows the protein with protease resistance, enabling efficient target screening and identification as a simple yet practical research tool. Our findings demonstrated that the rate of PDI degradation in PA-treated samples was notably diminished when compared with DMSO-exposed controls suggesting that PA can enhance the protease resistance of PDI through direct binding, thereby confirming that PDI is a target protein of PA (Figs. 5A and S3A). To explore the functional relevance of PDI in ulcerative colitis, we compared the expression levels between UC patients and healthy controls. The data revealed that PDI expression abundance in UC patients was markedly elevated relative to healthy individuals (P = 0.0071) (Fig. 5B). These findings suggest that PDI expression is regulated during the pathogenesis of UC.

As a core protein with multiple enzymatic activities in the endoplasmic reticulum, PDI is deeply involved in key physiological and pathological processes such as endoplasmic reticulum stress and oxidative stress, and its reductive activity plays an irreplaceable role in maintaining the functional homeostasis of the cellular endoplasmic reticulum. Given the vital significance of PDI's reductive activity, we further investigated the impact of PA on this activity, thereby providing experimental evidence for clarifying the mechanism of action of PA. The reductive activity of PDI can specifically cleave the disulfide bonds between the A and B chains of insulin, leading to the dissociation and subsequent aggregation of the insulin B chain. Based on this property, the insulin re-

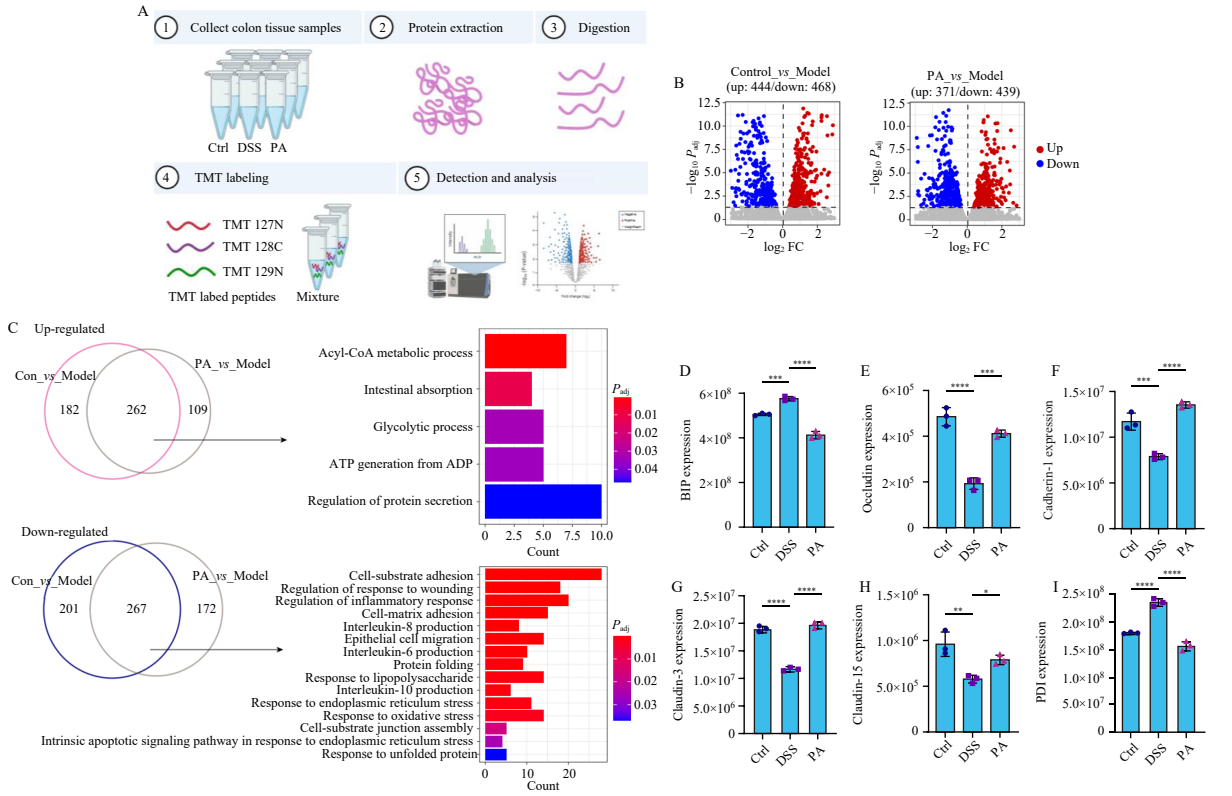

Fig. 4 Proteomic analysis of the colon in DSS-induced experimental colitis mice treated with PA. (A) Schematic diagram of the proteomics workflow. (B) Volcano plots of differentially expressed proteins (DEPs). (C) Venn diagrams and functional enrichment analysis of DEPs and GO biological process enrichment (top) and GO cellular component/biological process enrichment (bottom) of overlapping DEPs, colored by adjusted *P*-value (P_{adj}) and sized by gene count. (D–I) Quantitative analysis of proteomic data for key proteins: BIP (D), occludin (E), cadherin (F), claudin-3 (G), claudin-15 (H), and PDI (I). All experiments were conducted with 3 independent replicates per group. All data are presented as the mean ± SD. Statistical comparisons among multiple groups were performed using one-way ANOVA followed by Tukey's post-hoc test. Statistical significance: $^{*}P < 0.05$, $^{***}P < 0.001$, $^{****}P < 0.0001$ *vs* DSS group; ns, not significant.

duction assay is commonly used for the quantitative determination of PDI reductive activity. We next evaluated the reductase activity of PDI *in vitro* using both purified protein and cellular lysates. Results showed that PA treatment significantly suppressed PDI's reductase activity, implying that PA may modulate biological processes by regulating PDI's enzymatic function (Figs. 5C and 5D). To further characterize the protein interaction network involving PDI, we performed Co-IP WB analysis, which identified a specific interaction between PDI and IRE1. Interestingly, Co-IP assays revealed that PA treatment enhanced the interaction between PDI and IRE1 (Fig. 5E). This finding suggests that PA may act as a "molecular glue" to stabilize the PDI-IRE1 complex, locking IRE1 in a monomeric state and preventing its activation.

To explore whether modulation of this interaction underlies the protective actions of PA, we performed Western blot and RT-qPCR analyses. Previous studies have established that IRE1 activation involves dimerization, which stimulates its kinase and endonuclease activities [28]. In the present study, LPS treatment markedly promoted IRE1 dimerization, while PA administration effectively suppressed this process (Figs. 5F and 5G).

PA treatment also partially attenuated LPS-induced endoplasmic reticulum stress, with the high-dose PA group (PA-H) exhibiting a more pronounced protective response. RT-qPCR results indicated that LPS challenge markedly increased the mRNA abundance of *ire1* and *xbp1s*, and these levels were significantly reduced following PA treatment (Figs. 5H and 5I). Consistent with these findings, further mechanistic studies revealed that LPS induces endoplasmic reticulum stress, which drives the marked upregulation of key ER stress-associated molecules, including IRE1, BIP, CHOP, and XBP1s; importantly, this effect was reversed by PA treatment (Figs. 5J, 5K, and S3B–S3H). In summary, this study provides preliminary evidence that PA mitigates colitis by targeting PDI's reductase activity and alleviating IRE1-mediated endoplasmic reticulum stress, thereby exerting a protective effect.

3.6. PA ameliorates DSS-induced gut microbiota dysbiosis

The gut microbiota is essential for preserving intestinal microbial barrier integrity and sustaining host metabolic homeostasis. In this study, we systematically evaluated alterations in microbial composition and structure under different treatment conditions by collecting and analyzing fecal samples from mouse. An index of alpha diversity represented by the Shannon index revealed significant intergroup differences in community diversity (Figs. 6A–6D). Specifically, the DSS-group exhibited considerable fluctuations in microbial diversity, whereas treatment with varying doses of PA (PA-L and PA-H groups) differentially modulated diversity restoration. Notably, PA-L group demonstrated a more pronounced effect in restoring microbial diversity toward homeostasis.

Principal coordinate analysis (PCoA) further revealed structural divergence in microbial communities across groups, indicating that PA intervention may restore the microbial composition of the model group toward a normative profile through modulation of community architecture (Fig. 6E). Venn diagram analysis identified 383 bacterial species common to the CON, model, PA-L, and PA-H groups, suggesting the presence of a core microbiota that remains relatively stable under varying treatment conditions (Fig. 6F). Linear discriminant analysis (LDA) was employed to assess intergroup differences in microbial abundance, with taxonomic distributions visualized using evolutionary branching diagrams. In the model group, the phylum *Proteobacteria* (p_*Proteobacteria*) was significantly enriched, indicating that the gut microbiota was dominated by pathogenic taxa after DSS treatment. In the PA-H group, the *Verrucomicrobiota* branch corresponded to the genus *Akkermansia* (g_*Akkermansia*), which had a relat-

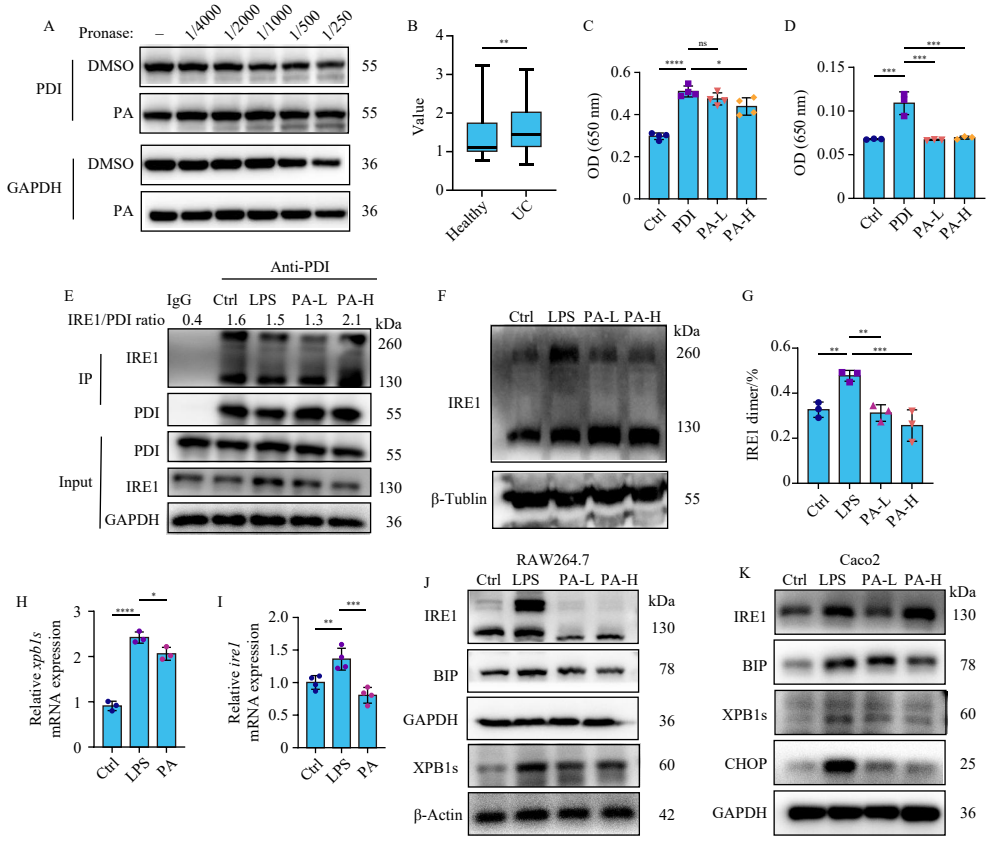

Fig. 5 PA exerts protective effects against UC by targeting PDI. (A) PDI protease resistance assay: assessed PDI conformational change after PA treatment, with GAPDH as loading control. (B) PDI expression in clinical samples: box plot of PDI levels in healthy controls (n = 31) and UC patients (n = 55), analyzed *via* the Mann-Whitney U test ($^{**}P < 0.01$ *vs* healthy control group). (C and D) PDI reductase activity assay. Activity measured in cell lysates (C) and recombinant PDI (D). (E) Co-IP assay: validated the interaction between PDI and IRE1. (F and G) IRE1 dimer WB and statistical analysis. (H and I) mRNA levels of *ire1* (H) and *xbp1s* (I). (J and K) WB of endoplasmic reticulum stress-related proteins IRE1, BIP, and XBP1s. Data are mean ± SEM from three independent experiments (n = 3–4). One-way ANOVA was performed, and significance was set at $^{*}P < 0.05$, $^{**}P < 0.01$, $^{***}P < 0.001$, $^{****}P < 0.0001$ *vs* LPS group or PDI group; ns, not significant.

ively high LDA score. This result confirms that PA at high doses can specifically enrich beneficial bacteria such as *Akkermansia* (Figs. S4A and 6G).

Specifically, in the Ctrl group, the dominant microbial communities were primarily concentrated in the phylum *Bacteroidetes*, including the class *Bacteroidia* (c_*Bacteroidia*), order *Bacteroidales* (o_*Bacteroidales*), and family *Muribaculaceae*. Additionally, dominant taxa included the family *Eggerthellaceae* (phylum *Actinobacteriota*), class *Chlamydobactria*, and class *Bacilli* (phylum *Firmicutes*). These groups represent the typical symbiotic core microbiota in healthy intestines, which participate in key physiological functions such as nutrient metabolism and intestinal barrier maintenance, suggesting that the microbial structure of the Ctrl group more closely resembles a healthy state. In the DSS group, dominant taxa were primarily from the phylum *Proteobacteria*, encompassing the class *γ-Proteobacteria* (c_*Gammaproteobacteria*), order *Enterobacteriales* (o_*Enterobacteriales*), and family *Enterobacteriaceae* (f_*Enterobacteriaceae*). Meanwhile, groups such as the genus *Romboutsia* (phylum *Firmicutes*) and family *Peptostreptococcaceae* were significantly enriched. These taxa predominantly consist of potential pathogens or opportunistic pathogens, indicating that DSS treatment may induce an imbalance in gut microbiota toward a pathogenic structure. In the PAL group, dominant microbiota was concentrated in the order *Oscillospirales* (phylum *Firmicutes*), with groups such as the family *Enterococcaceae* and order *Lactobacillales* also being dominant. *Lactobacillales*, a typical probiotic group, showed enrichment, suggesting that PA-L treatment may regulate gut microbiota by promoting the growth of probiotics. In the PA-H group, dominant taxa primarily included the genus *Akkermansia* and family *Akkermansiaceae* (phylum *Verrucomicrobiota*), as well as the order *Clostridia*_UCG_014 and family *Rikenellaceae* (phylum *Firmicutes*). *Akkermansia*, recognized as a beneficial bacterium, participates in maintaining the intestinal mucus layer and regulating metabolism. The enrichment of this group indicates that PA-H administration may facilitate the expansion of beneficial bacterial taxa, thereby reshaping the gut microbiota into a probiotic structure (Figs. 6H and 6I).

Consistent with previous findings, compared to the DSS model group, the Ctrl group exhibited significantly higher abundances of the genera *Lactobacillus*, *Muribaculum*, *Rikenella*, and *Parvibacter*. Similarly, the PA-H group showed significantly higher abundances of *Akkermansia*, *Bacteroides*, *Alistipes*, and *Rikenellaceae*_RC9_gut_group compared to the DSS group. Numerous studies [29, 30] have demonstrated that *Akkermansia* enhances intestinal barrier function and promotes mucosal repair. The increased abundance of such beneficial bacteria suggests that PA treatment improves DSS-induced gut microbiota dysbiosis by promoting the proliferation of beneficial taxa (Figs. 6J and 6K).

In summary, PA treatment effectively mitigates model-induced structural disruptions in the gut microbiota. The underlying mechanism may involve the suppression of pathogenic bacteria and the promotion of beneficial taxa, including *Akkermansia*, thereby contributing to the restoration of microbial homeostasis.

4. Discussion

UC is distinguished by pathological modifications that characteristically initiate in the rectum and propagate proximally in a continuous fashion along the colonic tract. A key hallmark of UC lies in the dysregulated triggering of mucosal immune responses, which perpetuates sustained intestinal inflammatory activity and

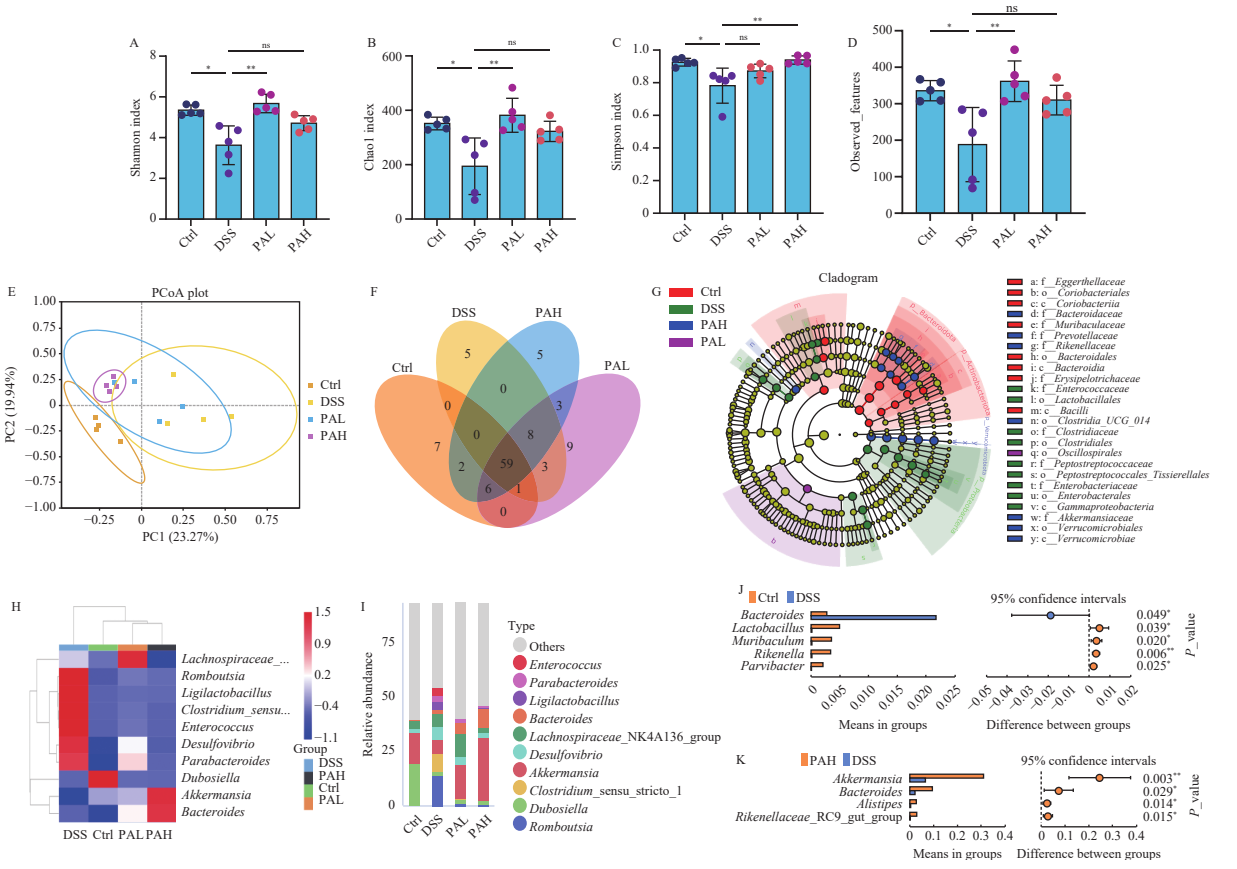

Fig. 6 PA ameliorates intestinal flora disorders in mice. (A–D) Alpha diversity analysis of gut microbiota: Shannon index (A), Chao1 index (B), Simpson index (C), and observed features (D). (E) Principal coordinate analysis (PCoA) based on Bray-Curtis distances, showing distinct separation of microbial community structures between groups. (F) Venn diagram displaying the overlap of differential bacterial taxa across Ctrl, DSS, PA-L, and PA-H groups. (G) LEfSe cladogram, identifying microbial taxa with significant differential abundance (LDA score > 2) among groups. Different colors represent taxa enriched in Ctrl (red), DSS (green), PA-H (yellow), and PA-L (purple) groups. (H) Heatmap of relative abundance of key bacterial genera, showing distinct clustering patterns of microbiota composition among groups. (I) Stacked bar plot showing the relative abundance of dominant bacterial genera in each group. (J and K) T-test analysis of differential bacterial genera: comparison of *Bacteroides*, *Lactobacillus*, and *Parabacteroides* between DSS and PA-H groups (J), and *Akkermansia*, *Alloprevotella*, and *Rikenellaceae*_RC9_gut_group between DSS and PA-H groups (K), with 95% confidence intervals for abundance differences. All experiments were performed with 5 mice per group ($n = 5$). Statistical evaluations for alpha diversity indices were conducted *via* ANOVA with subsequent Tukey's multiple comparisons test, while group dissimilarities in PCoA ordinations were assessed using the non-parametric Kruskal-Wallis procedure. Data are presented as mean ± SEM. Thresholds for statistical significance were defined as follows: $^{*}P < 0.05$, $^{**}P < 0.01$ *vs* DSS group; ns, not significant.

progressive tissue destruction. The pathogenesis of UC involves a complex interplay of three interconnected processes: compromised intestinal epithelial barrier integrity, gut microbiota dysbiosis, and aberrant immune signaling cascades [31, 32]. Current clinical management strategies primarily focus on controlling inflammatory symptoms and sustaining disease remission. However, their efficacy is often limited, with treatment response rates of only 20%–30% [33]. Thus, there is an urgent clinical need to develop effective, well-tolerated therapeutic agents with clearly elucidated mechanisms of action.

PA is a bioactive compound isolated from *Pogostemon cablin* (patchouli), and is a major component of the classic Chinese herbal formula Huoxiang Zhengqi San, which has been used for centuries to treat gastrointestinal disorders. While accumulating evidence [9, 10, 34] suggests that PA exerts a protective effect against UC, its precise molecular mechanisms of action remain incompletely elucidated.

Herein, we assessed the disease-alleviating efficacy of PA in a murine model of acute ulcerative colitis triggered by DSS. PA treatment significantly ameliorated weight loss, hematochezia, and colon shortening, and preserved intestinal epithelial integrity and goblet cell function. These findings confirm that PA exerts robust protective effects against colitis.

Subsequently, we employed a combination of proteomic profiling, 16S rRNA sequencing, WB, and RT-qPCR to elucidate the potential mechanisms underlying PA-mediated protection against UC, the result is shown in Fig. 7. Our findings reveal that PA may act as a potential molecular glue that stabilizes the PDI-IRE1 complex. Unlike conventional inhibitors that typically block protein-protein interactions, PA appears to enhance the binding between PDI and IRE1. This unique mode of action may lock IRE1 in a stable, inactive state by preventing its dissociation from PDI, thereby inhibiting IRE1 dimerization and downstream UPR signaling. This "locking" mechanism highlights a novel strategy for targeting the UPR pathway in UC therapy.

Within the human intestinal tract, the gut microbiome constitutes an intricately structured and taxonomically varied community, playing a pivotal role in maintaining intestinal homeostasis by regulating epithelial barrier function, immune responses, and microbial colonization resistance. For example, beneficial commensal bacteria can facilitate the generation of regulatory T cells to restrain aberrant inflammatory responses [35, 36]; in contrast, microbial dysbiosis may trigger immune dysregulation, which contributes to the onset and progression of disorders including inflammatory bowel disease [37]. In the present study, microbiome analysis showed that PA treatment reversed DSS-induced decreases in microbial diversity and significantly increased the relative abundance of *Akkermansia muciniphila*, a mucin-degrading bacterium associated with improved barrier function and reduced inflammation. These findings suggest that PA may exert its protective effects through dual mechanisms involving modulation of the gut microbiota and inhibition of ER stress *via* PDI targeting.

A key innovation of this study is the identification of a novel

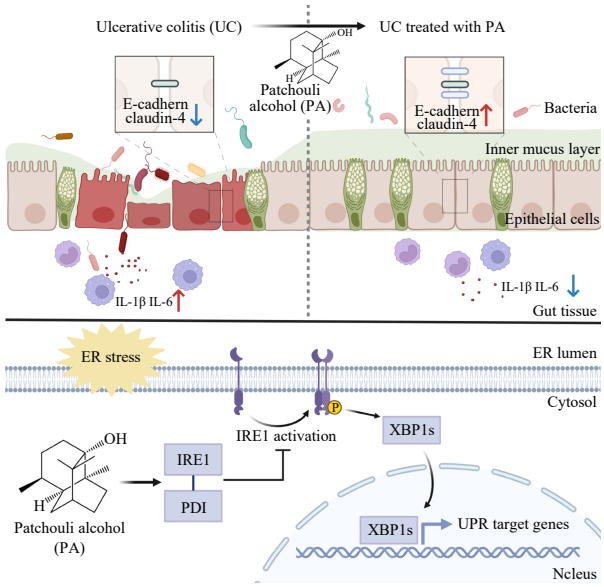

Fig. 7 Schematic diagram of the protective mechanism of PA against UC. PA targets the PDI-IRE1/XBP1s pathway to alleviate endoplasmic reticulum stress, thereby mitigating intestinal inflammation, reconstructing epithelial tight junctions and enriching beneficial gut microbiota.

interaction between PA, PDI, and IRE1. Specifically, we demonstrate that PA promotes the PDI-IRE1 interaction, thereby inhibiting IRE1 dimerization and downstream ER stress signaling. This mechanism is distinct from existing UC therapies and provides a new direction for developing PDI-targeted agents. While these results are encouraging, certain limitations merit consideration. To begin with, although the acute colitis model induced by DSS mirrors major pathological characteristics of UC, it does not fully recapitulate human chronic UC, particularly in terms of pathogenesis and disease progression. In addition, PDI was identified as a direct target of PA in the DARTS assay; however, this assay was associated with notable technical limitations. During the experimental procedure, the β-actin exhibited a more pronounced degradation pattern compared with PDI. We subsequently replaced the internal reference with GAPDH to re-evaluate protein stability, which partially mitigated the degradation issue but failed to completely eliminate this technical artifact. Thus, additional complementary experiments are warranted in future studies to further validate PDI as a bona fide target of PA. Next, although our preliminary data indicate that PA acts as a molecular glue to stabilize the PDI-IRE1 complex, the precise structural basis of this interaction and whether PA binds directly to PDI, IRE1, or their interface remains unclear. A further consideration is the mechanistic validation was predominantly conducted in the RAW264.7 macrophage cell line and Caco2 cells; additional studies using other disease-relevant cell types or organoid are required to comprehensively verify the universality of this pathway. To address these gaps, future studies should utilize multicellular co-culture models and conditional knockout animal models to fully clarify the involved mechanisms. Finally, while PA modulated the gut microbiota, including increasing *Akkermansia* abundance, the specific role of these microbial changes in PA's therapeutic effects and their link to ER stress regulation warrants further investigation.

5. Conclusions

In summary, the protective effect of PA against colitis is mediated by targeting PDI. PA acts as a potential molecular glue that stabilizes the PDI-IRE1 complex, thereby inhibiting IRE1 dimerization and attenuating ER stress. Additionally, PA modulates the gut microbiota to support intestinal barrier function. Collectively, these findings highlight PA as a promising therapeutic agent for UC with a distinct mechanism of action.

Funding

This work was supported by the GuangDong Basic and Applied Basic Research Foundation (No. 2025A1515011816) and the National Natural Science Foundation of China (Nos. 82305014, 82304827 and 82274387).

Supporting information

Supporting information for this work can be obtained by contacting the corresponding authors *via* E-mail.

Conflict of interest

The authors declare no conflicts of interest.

References

1 Le Berre C, Honap S, Peyrin-Biroulet L. Ulcerative colitis. *Lancet*. 2023;402 (10401):571-584. https://doi.org/10.1016/S0140-6736(23)00966-2.
2 Popov J, Caputi V, Nandeesha N, et al. Microbiota-immune interactions in ulcerative colitis and colitis associated cancer and emerging microbiota-based therapies. *Int J Mol Sci*. 2021;22(21):11365. https://doi.org/10.3390/ijms222111365.
3 Sun Y, Yuan S, Chen X, et al. The contribution of genetic risk and lifestyle factors in the development of adult-onset inflammatory bowel disease: a prospective cohort study. *Am J Gastroenterol*. 2023;118(3):511-522. https://doi.org/10.14309/ajg.0000000000002180.
4 Bressler B, Marshall JK, Bernstein CN, et al. Clinical practice guidelines for the medical management of nonhospitalized ulcerative colitis: the Toronto consensus. *Gastroenterology*. 2015;148(5):1035-1058.e3. https://doi.org/10.1053/j.gastro.2015.03.001.
5 Feuerstein JD, Moss AC, Farraye FA. Ulcerative colitis. *Mayo Clin Proc*. 2019;94(7):1357-1373. https://doi.org/10.1016/j.mayocp.2019.01.018.
6 Shehab M, Alrashed F, Alsayegh A, et al. Comparative efficacy of biologics and small molecule in ulcerative colitis: a systematic review and network meta-analysis. *Clin Gastroenterol Hepatol*. 2025;23(2):250-262. https://doi.org/10.1016/j.cgh.2024.07.033.
7 Leong W, Huang G, Liao W, et al. Traditional patchouli essential oil modulates the host's immune responses and gut microbiota and exhibits potent anti-cancer effects in $Apc^{Min/+}$ mice. *Pharmacol Res*. 2022;176:106082. https://doi.org/10.1016/j.phrs.2022.106082.
8 Zrieq R, Ahmad I, Snoussi M, et al. Tomatidine and patchouli alcohol as inhibitors of SARS-CoV-2 enzymes (3CLpro, PLpro and NSP15) by molecular docking and molecular dynamics simulations. *Int J Mol Sci*. 2021;22(19):10693. https://doi.org/10.3390/ijms221910693.
9 Qu C, Yuan ZW, Yu XT, et al. Patchouli alcohol ameliorates dextran sodium sulfate-induced experimental colitis and suppresses tryptophan catabolism. *Pharmacol Res*. 2017;121:70-82. https://doi.org/10.1016/j.phrs.2017.04.017.
10 Wu J, Gan Y, Li M, et al. Patchouli alcohol attenuates 5-fluorouracil-induced intestinal mucositis *via* TLR2/MyD88/NF-κB pathway and regulation of microbiota. *Biomed Pharmacother*. 2020;124:109883. https://doi.org/10.1016/j.biopha.2020.109883.
11 Han H, Gao M, Wang F, et al. Protective effects of patchouli alcohol against DSS-induced ulcerative colitis. *Sci Rep*. 2024;14(1):16745. https://doi.org/10.1038/s41598-024-66259-8.
12 Wang C, Li W, Ren J, et al. Structural insights into the redox-regulated dynamic conformations of human protein disulfide isomerase. *Antioxid Redox Signal*. 2013;19(1):36-45. https://doi.org/10.1089/ars.2012.4630.
13 Yang S, Wang X, Cui L, et al. Compact conformations of human protein disulfide isomerase. *PLoS One*. 2014;9(8):e103472. https://doi.org/10.1371/journal.pone.0103472.
14 Klappa P, Ruddock LW, Darby NJ, et al. The b' domain provides the principal peptide-binding site of protein disulfide isomerase but all domains contribute to binding of misfolded proteins. *EMBO J*. 1998;17(4):927-935. https://doi.org/10.1093/emboj/17.4.927.
15 Bendapudi PK, Bekendam RH, Lin L, et al. ML359, a small molecule inhibitor of protein disulfide isomerase that prevents thrombus formation and inhibits oxidoreductase but not transnitrosylase activity. *Blood*. 2014;124 (21):2880. https://doi.org/10.1182/blood.V124.21.2880.2880.
16 Jasuja R, Passam FH, Kennedy DR, et al. Protein disulfide isomerase inhibitors constitute a new class of antithrombotic agents. *J Clin Invest*. 2012;122(6):2104-2113. https://doi.org/10.1172/JCI61228.
17 Hung CS, Lee KL, Huang WJ, et al. Pan-inhibition of protein disulfide isomerase caused cell death through disrupting cellular proteostasis in pancreatic ductal adenocarcinoma cells. *Int J Mol Sci*. 2023;24(22):16467. https://doi.org/10.3390/ijms242216467.
18 Kim HT, Russell RL, Raina AK, et al. Protein disulfide isomerase in Alzheimer disease. *Antioxid Redox Signal*. 2000;2(3):485-489. https://doi.org/10.1089/15230860050192260.

19 Ono S, Ogura J, Sugiura H, et al. Glutathione depletion results in S-nitrosylation of protein disulfide isomerase in neuroblastoma cells. *Life Sci*. 2023;316:121442. https://doi.org/10.1016/j.lfs.2023.121442.
20 Qian C, Hu C, Xu Y, et al. Intestinal epithelial-derived USP13 alleviates colonic inflammation by suppressing GRP78-mediated endoplasmic reticulum stress. *Adv Sci*. 2025;12(38):e00741. https://doi.org/10.1002/advs.202500741.
21 Yuan S, She D, Jiang S, et al. Endoplasmic reticulum stress and therapeutic strategies in metabolic, neurodegenerative diseases and cancer. *Mol Med*. 2024;30(1):40. https://doi.org/10.1186/s10020-024-00808-9.
22 Coelho JP, Feige MJ. In case of stress, hold tight: phosphorylation switches PDI from an oxidoreductase to a holdase, tuning ER proteostasis. *EMBO J*. 2020;39(10):e104880. https://doi.org/10.15252/embj.2020104880.
23 Yu J, Li T, Liu Y, et al. Phosphorylation switches protein disulfide isomerase activity to maintain proteostasis and attenuate ER stress. *EMBO J*. 2020;39(10):e103841. https://doi.org/10.15252/embj.2019103841.
24 Shergalis AG, Hu S, Bankhead A, et al. Role of the ERO1-PDI interaction in oxidative protein folding and disease ERO1-PDI. *Pharmacol Ther*. 2020;210:107525. https://doi.org/10.1016/j.pharmthera.2020.107525.
25 Armstrong DA, Major JA, Chudyk A, et al. Neutrophil chemoattractant genes *KC* and *MIP-2* are expressed in different cell populations at sites of surgical injury. *J Leukoc Biol*. 2004;75(4):641-648. https://doi.org/10.1189/jlb.0803370.
26 Zhang Q, Luo P, Xia F, et al. Capsaicin ameliorates inflammation in a TRPV1-independent mechanism by inhibiting PKM2-LDHA-mediated Warburg effect in sepsis. *Cell Chem Biol*. 2022;29(8):1248-1259.e6. https://doi.org/10.1016/j.chembiol.2022.06.011.
27 Zhu Y, Wang L, Li J, et al. Photoaffinity labeling coupled with proteomics identify PDI-ADAM17 module is targeted by (−)-vinigrol to induce TNFR1 shedding and ameliorate rheumatoid arthritis in mice. *Cell Chem Biol*. 2024;31(3):452-464.e10. https://doi.org/10.1016/j.chembiol.2023.10.003.
28 Belyy V, Zuazo-Gaztelu I, Alamban A, et al. Endoplasmic reticulum stress activates human IRE1α through reversible assembly of inactive dimers into small oligomers. *eLife*. 2022;11:e74342. https://doi.org/10.7554/elife.74342.sa0.
29 Chelakkot C, Choi Y, Kim DEK, et al. *Akkermansia muciniphila*-derived extracellular vesicles influence gut permeability through the regulation of tight junctions. *Exp Mol Med*. 2018;50(2):e450. https://doi.org/10.1038/emm.2017.282.
30 Shuoker B, Pichler MJ, Jin C, et al. Sialidases and fucosidases of *Akkermansia muciniphila* are crucial for growth on mucin and nutrient sharing with mucus-associated gut bacteria. *Nat Commun*. 2023;14(1):1833. https://doi.org/10.1101/2022.09.10.507281.
31 Kayama H, Okumura R, Takeda K. Interaction between the microbiota, epithelia, and immune cells in the intestine. *Annu Rev Immunol*. 2020;38(1):23-48. https://doi.org/10.1146/annurev-immunol-070119-115104.
32 Zhao MA, Chu J, Feng S, et al. Immunological mechanisms of inflammatory diseases caused by gut microbiota dysbiosis: a review. *Biomed Pharmacother*. 2023;164:114985. https://doi.org/10.1016/j.biopha.2023.114985.
33 Alsoud D, Verstockt B, Fiocchi C, et al. Breaking the therapeutic ceiling in drug development in ulcerative colitis. *Lancet Gastroenterol Hepatol*. 2021;6(7):589-595. https://doi.org/10.1016/S2468-1253(21)00065-0.
34 Chen W, Li T, Lin Y, et al. Patchouli alcohol restores gut homeostasis in irritable bowel syndrome with diarrhea through myosin Va-mediated neurotransmitter regulation. *Phytomedicine*. 2025;141:156681. https://doi.org/10.1016/j.phymed.2025.156681.
35 Dwivedi M, Kumar P, Laddha NC, et al. Induction of regulatory T cells: a role for probiotics and prebiotics to suppress autoimmunity. *Autoimmun Rev*. 2016;15(4):379-392. https://doi.org/10.1016/j.autrev.2016.01.002.
36 Verma R, Lee C, Jeun EJ, et al. Cell surface polysaccharides of *Bifidobacterium bifidum* induce the generation of Foxp3$^+$ regulatory T cells. *Sci Immunol*. 2018;3(28):eaat6975. https://doi.org/10.1126/sciimmunol.aat6975.
37 Sharma B, Agriantonis G, Twelker K, et al. Gut microbiota serves as a crucial independent biomarker in inflammatory bowel disease (IBD). *Int J Mol Sci*. 2025;26(6):2503. https://doi.org/10.3390/ijms26062503.